Preprints (www.preprints.org) | NOT PEER-REVIEWED | Posted: 22 January 2019 doi:10.20944/preprints201901.0222.v1

Peer-reviewed version available at *J. Mar. Sci. Eng.* **2019**, *7*, 71; doi:10.3390/jmse7030071

Article

The Efficient Application of an Impulse Source Wavemaker to CFD Simulations

Pál Schmitt [1]*, Christian Windt [2] Josh Davidson [2], John V. Ringwood [2] and Trevor Whittaker[1]

[1] Marine Research Group, Queen's University Belfast, BT9 5AG Belfast, Northern Ireland; p.schmitt@qub.ac.uk
[2] Centre for Ocean Energy Research, Maynooth University, Ireland; e-mail@e-mail.com
* Correspondence: p.schmitt@qub.ac.uk;

Version January 22, 2019 submitted to Preprints

Abstract: Computational Fluid Dynamics (CFD) simulations, based on Reynolds Averaged Navier Stokes (RANS) models, are a useful tool for a wide range of coastal and offshore applications, providing a high fidelity representation of the underlying hydrodynamic processes. Generating input waves in the CFD simulation is performed by a numerical wavemaker (NWM), with a variety of different NWM methods existing for this task. While NWMs, based on impulse source methods, have been widely applied for wave generation in depth averaged, shallow water models, they have not seen the same level of adoption in the more general RANS based CFD simulations, due to difficulties in relating the required impulse source function to the resulting free surface elevation for non-shallow water cases. This paper presents an implementation of an impulse source wavemaker, which is able to self-calibrate the impulse source function to produce a desired wave series in deep or shallow water at a specific point in time and space. Example applications are presented, for a numerical wave tank (NWT), based on the opensource CFD software OpenFOAM, for wave packets in deep and shallow water, highlighting the correct calibration of phase and amplitude. Also, the suitability for cases requiring very low reflection from NWT boundaries is demonstrated. Possible issues in the use of the method are discussed and guidance for good application is given.

Keywords: numerical wave tank; internal wavemaker; CFD ; wave generation; OpenFOAM

---

1. Introduction

While CFD enables the simulation of complex flow phenomena, such as two-phase flows and gravity waves, setting up a simulation of coastal or marine engineering processes, with correct wave creation and minimum reflection, can be a challenge. A wide range of NWM methods exist in the literature for the generation and absorption of waves in a CFD simulation.

Wave generation methods can be broadly grouped into two main categories:

1. Replication of physical wavemakers, such as oscillating flaps, paddles or pistons
2. Implementation of numerical/mathematical techniques, introducing source terms or similar into the governing equations

The first category of wave generation methods directly simulates the wavemaker by a moving wall, requiring mesh motion/deformation in the CFD domain [**?**], which can be a complex and computationally expensive task. Additionally, because these methods replicate the real processes in a physical laboratory tank, they also incur the well known drawbacks of physical wavemakers encountered in an experimental facility, such as evanescent waves, imperfect wave absorption and the required implementation of a wavemaker control system. Another drawback of conventional wave pistons is that they are typically limited to low order waves (first or second order).

© 2019 by the author(s). Distributed under a Creative Commons CC BY license.

Preprints (www.preprints.org) | NOT PEER-REVIEWED | Posted: 22 January 2019 doi:10.20944/preprints201901.0222.v1

Peer-reviewed version available at J. Mar. Sci. Eng. 2019, 7, 71; doi:10.3390/jmse7030071

In contrast to directly mimicking physical wavemakers, the second category of wave generation methods are generally more computationally efficient, using numerical algorithms to create the desired flow conditions by manipulating the field variables. In principle there are four types of methods in the second category of wave generators:

- *relaxation method* - relaxes the results of the simulation inside the domain with the results given by wave theory [**? ? ? ?**] (linear or higher order) or other numerical models like boundary element methods (BEM) for example [**? ?**].
- *boundary method* - creates and absorbs waves on boundary patches through Dirichlet boundary conditions [**? ? ?**]
- *mass source method* - the wave is created by adding a source term to the continuity equation [**? ? ? ?**]
- *impulse source method* - the wave is created by adding a source term to the impulse equation [**? ? ? ?**]

Correspondingly, wave absorption can also be achieved using a number of methods. The trivial solution, of using a very long tank and limiting the simulation duration to a small number of wave cycles, is certainly not efficient or elegant and will therefore not be considered herein. The relaxation and boundary wave generation methods, allow for wave absorption to be achieved actively by the NWM, whereas the mass and impulse source function methods can be used in combination with numerical beaches to dissipate waves and eliminate reflections.

1.1. Impulse source wavemaker

While a comparison of different wavemakers is not within the scope of this paper, we want to highlight some common issues in NWTs. Wavemakers relying on open boundaries or algorithms that set the species variable, such as relaxation methods, are not necessarily mass conservative. Compared to an experimental facility, where waves are typically created in an enclosed volume of water, wave run-up along a sloping bottom, for example, might not be recreated correctly. Numerical beaches, while in many cases expected to be more computationally expensive than boundary conditions, are able to absorb waves to any desired level of reflection. The user thus has a possibility to balance computational burden against permissible reflections. Mass source methods are very similar to impulse source methods, but problems can arise when generating waves of significant height in shallow water. Once the surface level falls below the source region, wave generation fails. It should be noted that, at the wavemaker location, the surface elevation is twice the wave amplitude of the target wave train, since two wave trains travelling in opposite direction are created. The present paper thus focuses on the impluse source wavemaker.

The difficulty, in utilising an impulse source as a NWM, is in calculating the required source function to obtain a desired target wave series. Since the free surface is not a variable in the RANS equations, there is no direct expression relating the impulse source function to the resulting generated wave series. However, for depth-integrated equations, the free surface does appear as a variable, which [**?**] utilised to derive a transfer function between the source amplitude and the surface wave characteristics, generating mono- and polychromatic waves in Boussinesq-type wave models. Following this approach, generating waves by manipulating the impulse term in the Navier Stokes equation has successfully been applied to shallow water waves in CFD simulations in [**? ?**]. [**?**] describe several issues, especially when creating deep water waves, originating from the Boussinesq simplifications used in the source term derivation. They also discuss limitations inducing numerical errors when applying a momentum source function to random wave generation. Despite those promising first steps, internal wavemakers have not seen widespread application.

In theory, limitations due to the Boussinesq simplification might be overcome by employing stream functions or other high order wave theories. In practice, evaluating higher order wave theories at multiple spatial positions (across all faces of the patch or all cells in the wavemaker region) can be computationally

Preprints (www.preprints.org) | NOT PEER-REVIEWED | Posted: 22 January 2019 doi:10.20944/preprints201901.0222.v1

Peer-reviewed version available at J. Mar. Sci. Eng. 2019, 7, 71; doi:10.3390/jmse7030071

expensive. Furthermore, in many practical CFD applications the accurate wave trace description is required at some distance away from the wave maker, typically in the middle of the domain. [?] presented some progress in the use of neural networks for calibrating extreme waves in shallow water conditions.

The present paper follows an alternative, more generalised, method to determine the required source function. The proposed method follows from standard calibration procedures utilised for physical wavemakers in real wave tanks, which iteratively tune the input signal applied to the wavemaker in order to minimise the error between the measured and targeted wave series. Unlike previous methods to determine the source function, which are restricted to shallow water waves, the method proposed herein is applicable from deep to shallow water conditions, able to generate any realistic wave series at any desired location in a NWT, without explicitly employing any wave theory whatsoever. Additionally, while disipation can reduce a theoretically correct wave height from the source region as it travels to the target location, the proposed method overcomes this problem since it is designed to obtain the desired wave signal at the target location.

Iterative calibration methods will of course increase the computational burden when compared directly to an analytically derived accurate wavemaker function. However, by performing the calibration runs on a two dimensional slice, the computational overhead is almost negligible compared to fully three dimensional simulations of realistic test cases. Applying a calibrated two dimensional result to a corresponding three dimensional domain is efficient and has also been the recommended approach by [?].

The paper will demonstrate that, by utilising the proposed method, the source function can consist of a purely horizontal impulse component which varies in time. The time evolution of the magnitude and direction of this simple impulse source term can be calibrated using a standard spectral analysis method, which is commonly used in physical wave tanks. The remaining parameters of the impulse source wavemaker that need to be chosen are then the geometrical size and shape of the source function inside the NWT domain. An investigation of the effect of these geometric parameters will be presented to offer guidance on the selection of those values.

1.2. Outline of paper

The remainder of the paper is organised in the following four sections. In Section **??** the implementation of the impulse source wavemaker and the theoretical background is discussed in detail. The following two sections then present the application of the impulse source wavemaker to a wave packet in deep and shallow water conditions, with Section **??** detailing the particulars of the case study, and Section **??** presenting the results and a discussion. Finally, in Section **??**, a number of conclusions are drawn.

2. Implementation

This section details the implementation of the impulse source wavemaker, within a CFD solver, based on RANS models. First, the modification of the impulse equation to produce the wavemaker is detailed. Next, setting the parameter values associated with the modified impulse equation is discussed. Finally, the calibration procedure used to generate a target wave at a specified location is presented.

2.1. The impulse equation

A RANS model includes the following impulse equation:

$$\frac{\partial(\rho\mathbf{U})}{\partial t} + \nabla\cdot(\rho\mathbf{U}\mathbf{U}) = -\nabla p + \nabla\cdot\mathbf{T} + \rho\mathbf{F}_b \qquad (1)$$

Preprints (www.preprints.org) | NOT PEER-REVIEWED | Posted: 22 January 2019 doi:10.20944/preprints201901.0222.v1

Peer-reviewed version available at J. Mar. Sci. Eng. 2019, 7, 71; doi:10.3390/jmse7030071

where t is time, $\mathbf{U}$ the fluid velcoity, p the fluid pressure, ρ the fluid density, $\mathbf{T}$ the stress tensor and $\mathbf{F}_b$ the external forces such as gravity. The stress tensor can include terms from a turbulence model, however for this paper all cases presented use a laminar flow model because the waves are non breaking. The current impulse source wavemaker is implemented by adding two terms to Eq. (**??**):

- $r\rho\mathbf{a}_{wm}$: This is the source term used for wave generation, where r is a scalar variable that defines the wavemaker region and $\mathbf{a}_{wm}$ is the acceleration input to the wavemaker at each cell centre within r.
- $sand\rho\mathbf{U}$: This describes a dissipation term used to implement a numerical beach, where the variable field *sand* controls the strength of the dissipation, equalling zero in the central regions of the domain where the working wavefield is required and then gradually increasing towards the boundary over the length of the numerical beach [**?**].

Introducing these two terms to Eq. (**??**), yields the adapted impulse equation:

$$\frac{\partial(\rho\mathbf{U})}{\partial t} + \nabla\cdot(\rho\mathbf{U}\mathbf{U}) = -\nabla p + \nabla\cdot\mathbf{T} + \rho\mathbf{F}_b + r\rho\mathbf{a}_{wm} + sand\rho\mathbf{U} \tag{2}$$

2.2. Setting parameter values

The values for the parameter fields r and *sand* are set during preprocessing and their definition is crucial for the correct functioning of the method.

- r is set to 1 in the region where the wavemaker exists, and 0 everywhere else in the NWT domain. Therefore, the size of the wavemaker and its position within the NWT must also be selected. To offer guidance on the selection of the wavemaker size and position, the case study presented in Sections **??** and **??**, investigates the effect of these parameters on the wavemaker performance.
- *sand* is initialised using an analytical expression relating the value of *sand* and the geometric coordinates of the NWT. The simplest expression would be a step function, where the value of *sand* is constant inside the beach and is zero everywhere else in the NWT. However, such sharp increase in the dissipation will cause numerical reflections. Instead, the value of *sand* should be increased gradually from the start to the end of the numerical beach. Eq. (**??**) is used in the current implementation which has been shown to produce good absorption [**?**]:

$$\begin{aligned} sand(x) = -2\cdot sand_{Max}\left(\frac{(l_{beach}-x)}{l_{beach}}\right)^3 + \\ 3\cdot sand_{Max}\left(\frac{(l_{beach}-x)}{l_{beach}}\right)^2 \end{aligned} \tag{3}$$

where l_{beach} is the length of the numerical beach, x is the position within the numerical beach, equalling zero at the start and increasing to l_{beach} at the NWT wall, and $sand_{Max}$ stands for the maximum value of *sand*. Guidance on the selection of the parameters l_{beach} and $sand_{Max}$ is also given in the case study (see Section **??**).

[**?**] recently derived an analytical solution describing the ideal setting for *sand* and validated the method in a numerical experiment, removing the need for parameter studies in the future.

2.3. Calibration procedure

The source acceleration, $\mathbf{a}_{wm}(t)$, is calibrated, using a standard spectral analysis method, based on work presented in [**?**], to produce a target wave series at a desired position within the NWT. Figure **??** shows a schematic of the calibration procedure, which comprises the following steps:

Preprints (www.preprints.org) | NOT PEER-REVIEWED | Posted: 22 January 2019 doi:10.20944/preprints201901.0222.v1

Peer-reviewed version available at J. Mar. Sci. Eng. 2019, 7, 71; doi:10.3390/jmse7030071

1. Define target wave series at desired NWT location, $\eta_T(t)$, with a signal length $\mathscr{L}$ and $\mathscr{N}$ samples
2. Perform a Fast Fourier Transform (FFT) on $\eta_T(t)$, to obtain the amplitudes, $A_T(f_j)$, and phase components, $\phi_T(f_j)$, for each frequency component, f_j, with $j = \{1, 2, ..., \frac{\mathscr{N}}{2}\}$, where $f_1 = \frac{0}{\mathscr{L}}, f_2 = \frac{1}{\mathscr{L}}, ..., f_{\mathscr{N}} = \frac{\mathscr{N}}{2\mathscr{L}} - \frac{1}{\mathscr{L}}$
3. Generate an initial time series for the wavemaker source term, $\mathbf{a}_{wm,1}(t)$ (can be chosen randomly or informed by $\eta_T(t)$)
4. Perform a FFT on $\mathbf{a}_{wm,1}(t)$, to obtain the amplitudes, $A_{a,1}(f_j)$, and phase components, $\phi_{a,1}(f_j)$, for each frequency component of the input source term
5. Run simulation, for iteration i, using the wavemaker source term $\mathbf{a}_{wm,i}(t)$, and measure the resulting free surface elevation at the chosen NWT location, $\eta_{R,i}(t)$
6. Perform a FFT on $\eta_{R,i}(t)$, to obtain the amplitudes, $A_{R,i}(f_j)$, and phase components, $\phi_{R,i}(f_j)$, for each frequency component of the generated wave series
7. Calculate the new amplitudes for each frequency component of the input source term, $A_{a,i+1}(f_j)$, by scaling the previous amplitudes, $A_{a,i}(f_j)$, with the ratio of target surface elevation amplitude, $A_T(f_j)$, and the generated surface elevation amplitude from the previous run, $A_{R,i}(f_j)$:
   - $A_{a,i+1}(f_j) = \frac{A_T(f_j)}{A_{R,i}(f_j)} A_{a,i}(f_j)$
8. Calculate the new phase components, $\phi_{a,i+1}(f_j)$, by summing $\phi_{a,i}(f_j)$ with the difference between the target elevation phase, $\phi_T(f_j)$, and the measured surface elevation phase from the previous run, $\phi_{R,i}(f_j)$:
   - $\phi_{a,i+1}(f_j) = \phi_{a,i}(f_j) + [\phi_T(f_j) - \phi_{R,i}(f_j)]$
9. Generate the new time series for the wavemaker source term, $\mathbf{a}_{wm,i+1}(t)$, by performing an Inverse Fourier Transform on $A_{a,i+1}(f_j)$ and $\phi_{a,i+1}(f_j)$
10. Repeat steps 5 - 9 until either a maximum number of iterations, or a threshold for the mean-squared error (MSE) between the target and resulting surface elevation, is reached.

It should be noted, that although the method is based on the work described by [**?**], we have further simplified it. Instead of evaluating the phase-shift caused by the distance between the wavemaker and the point of interest, which would require the use of some wave theory to find the wavenumber k, we directly adjust the phase between wavemaker and target (Step 8).

2.4. Calibration procedure for regular waves

The calibration method detailed above might fail to resolve the single peak in frequency domain for short time traces of regular waves. At the same time, in regular waves the phase of the wave is generally not of interest, allowing for a simplification of the calibration . [**? ? ?**] used the same solver formulation and simply tuned the amplitude of an oscillating source to create monochromatic waves of a desired height. The following calibration method is used for regular waves:

1. The source term is set to oscillate in horizontal direction with the desired wave frequency.
2. The amplitude $A_{a,i}$ is initialised with an arbitrary value.
3. After the initial, and each subsequent run, the surface elevation is analysed in time domain. The mean is removed from the surface elevation. Mean wave height $H_{R,i}$ is then obtained as the difference between the mean of the positive and mean of the negative peaks.
4. A new wave maker amplitude $A_{a,i+1}$ is obtained by linearly scaling the previous value with the ratio of target H_T and result wave height H_R as follows $A_{a,i+1} = \frac{H_T}{H_{R,i}} A_{a,i}$

Steps 3 and 4 are repeated until the desired wave height is achieved.

Peer-reviewed version available at J. Mar. Sci. Eng. 2019, 7, 71; doi:10.3390/jmse7030071

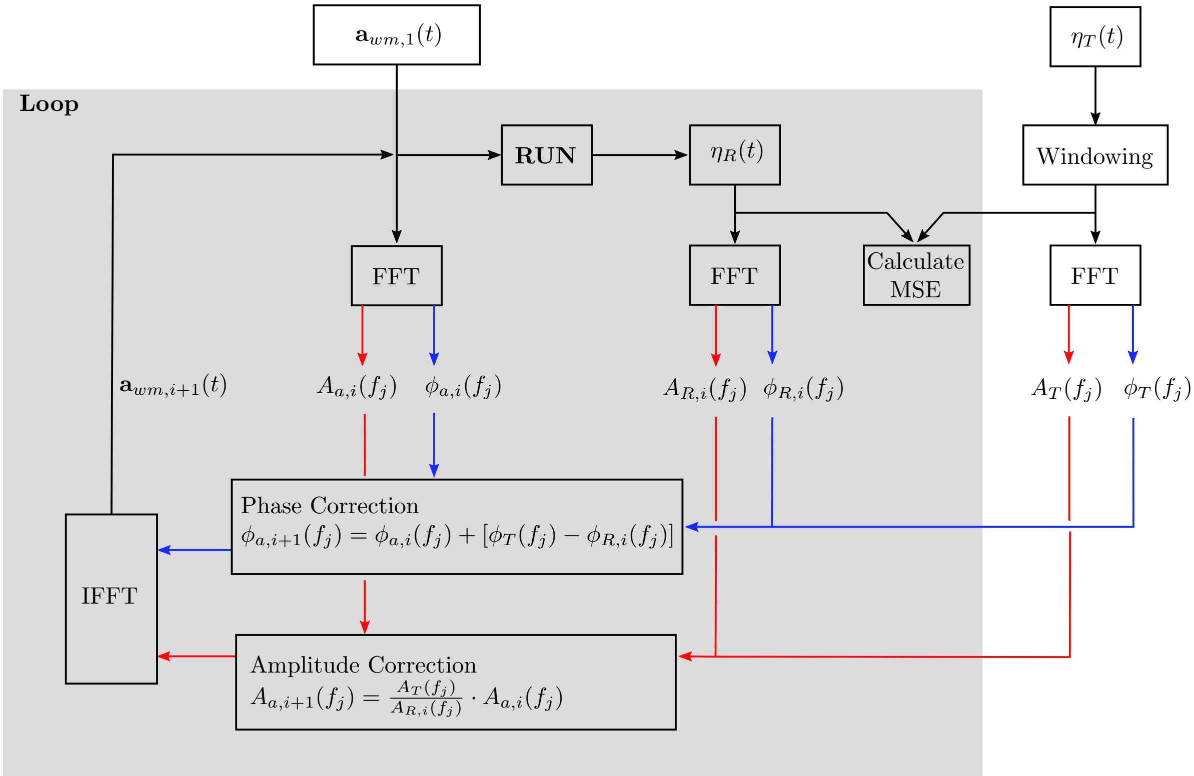

Figure 1. Schematic of the Calibration Method

3. Case study

A case study is now presented with two main objectives, firstly to demonstrate the capabilities of the impulse wavemaker and the self-calibration procedure in producing any realistic deep or shallow water wave series at a specified location in a wave tank. The second objective is to provide guidance on the selection of the wavemaker source region, by investigating the effect that the size and position of the source region has on the resulting waves. It might be expected that a very long source area will decrease accuracy, whereas a very short source region will require very large velocity components to create a target wave. For the shallow water impulse wavemaker in [?], a source length of about a quarter to half a wavelength is recommended. In shallow water, the entire water column, from the sea floor up to the water surface, performs an oscillating motion, whereas in deep water only part of the water column is affected and the wave motion does not extend to the sea floor. It is thus an interesting question how to choose the length and depth of the source region to achieve optimal results in deep, as well as shallow, water.

3.1. Target waves

The case study considers two types of target waves, multi-frequency and regular waves, to demonstrate the calibration procedures outlined in Sections **??** and **??**, respectively.

3.1.1. Multi-frequency wave packet

To demonstrate the ability of the impulse wavemaker, the case study creates a unidirectional multi-frequency wave packet at a specified location in the NWT. The wave packet considered is a realisation of the NewWave formulation as presented in [?]. A NewWave wave packet comprises a summation of all

Preprints (www.preprints.org) | NOT PEER-REVIEWED | Posted: 22 January 2019 doi:10.20944/preprints201901.0222.v1

Peer-reviewed version available at *J. Mar. Sci. Eng.* **2019**, *7*, 71; doi:10.3390/jmse7030071

the frequency components of a given spectrum, such that the largest amplitude wave crest is created in the temporal centre of the packet. The governing equations for the surface elevation, $\eta_T(t)$, and amplitude of each wave component, a_k, with $k = 1, ..., \mathscr{K}$, are given in Eq. (**??**) and (**??**), respectively:

$$\eta_T(t) = \sum_{k=1}^{\mathscr{K}} a_k cos\left[k_k(x - x_0) - \omega_k(t - t_0)\right] \tag{4}$$

$$a_k = A_0 \frac{S(f_k)\Delta f}{\sum_k^{\mathscr{K}} S(f_k)\Delta f} \tag{5}$$

In Eq. (**??**), x_0 represents the spatial focal location and t_0 the temporal focal instant. In Eq. (**??**), $S(f)$ is the spectral density and Δf the frequency step. A_0 represents the amplitude of the largest wave crest. For this case study, $A_0 = 0.02\,\mathrm{m}$, $\Delta f = 0.1\,\mathrm{s}^{-1}$, and $T_p = 1.1\,\mathrm{s}$ for the shallow case, contrasted with $T_p = 0.977\,\mathrm{s}$ for the deep water case. The different peak periods are chosen such that the peak wavelength, λ_p of 1.48 m remains identical across cases, yielding kh parameters of 1.06 for the shallow and 3.13 for the deep water case.

Although the parameters used in this case study are somewhat arbitrarily chosen, wave packets are generally well suited for testing the calibration of amplitudes and phases of different frequency components [**?**], and are also of practical relevance in industrial applications [**?**]. Time traces for the surface elevation $\eta(t)$, and plots of the spectra density $S(f)$ for the shallow and deep water case, are shown in Fig. **??**.

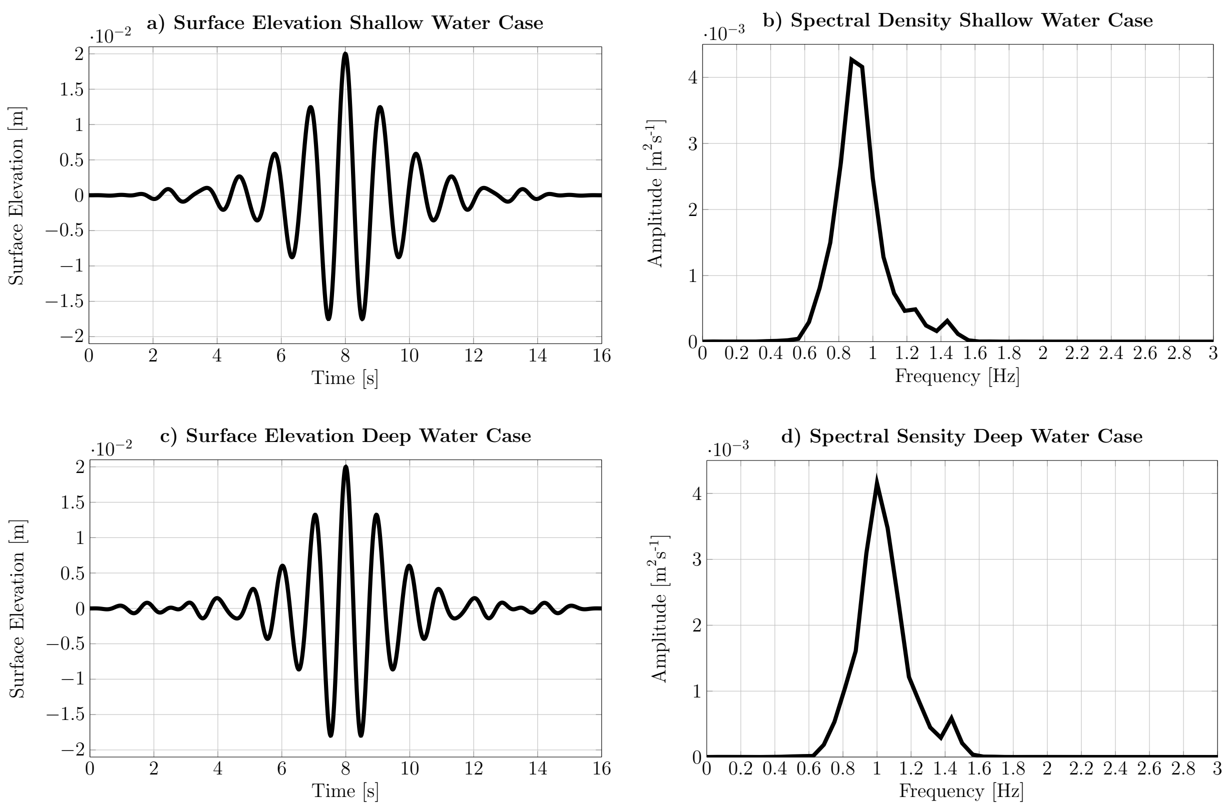

Figure 2. Target wave packet for the impulse wave maker to produce in the case study: Surface elevation (a), c)) and spectral density (b), d)) for the shallow and deep water case

Preprints (www.preprints.org) | NOT PEER-REVIEWED | Posted: 22 January 2019 doi:10.20944/preprints201901.0222.v1

Peer-reviewed version available at J. Mar. Sci. Eng. 2019, 7, 71; doi:10.3390/jmse7030071

3.1.2. Regular waves

Two cases demonstrating the creation of regular waves in shallow and deep water are presented. The target wave height was set to $0.037m$ and the period to $1.1s$ for the shallow water case and $0.977s$ for the deep water case, replicating the peak frequency and maximum wave height of the corresponding wave packets described in Section **??**. If not mentioned specifically the settings found to be suitable for the corresponding wave packets have been used for the setup of these regular wave cases.

3.2. Source region

A rectangular shaped source region is used for all simulations, whose length, L, and height, H, are varied to investigate the effect of the source region size on the wave maker performance. Additionally, to investigate the effect of the position of the wavemaker within the water column, the depth of the source region is varied.

3.3. Simulation platform

The NWT implementation for this case study is based on the *interFoam* solver from the OpenFOAM toolbox. The *interFoam* solver uses a volume of fluid (VOF) approach for modelling the two different fluid phases, air and water, in order to capture and track and the free surface. More details on this solver can be found in [**?**]. Although the case study employs OpenFOAM as the CFD solver, the method can easily be applied to any CFD software that allows user coding. For example, [**?**] implements the shallow water impulse source wavemaker in ANSYS Fluent, using its user-defined functions capability.

The calibration function was implemented in the free scientific programming software, GNU Octave [**?**]. This results in all of the software utilised in this case study being opensource or free. The source code for the case study set-up and implementation has been shared by the authors on the CCP-WSI repository [**?**], allowing anyone to easily access and utilise the developed impulse source wavemaker.

3.4. Numerical wave tank set-up

Since the case study considers a unidirectional input wave, a two-dimensional (2D) NWT is implemented to simplify the set-up and reduce computational overheads. The NWT set-up is described below, detailing the geometry, boundary conditions, mesh and calibration of the absorption beach.

3.4.1. Geometry

The NWT geometry is depicted in Figure **??**. The depth of the NWT is set to 0.25 m for the shallow water case, and 0.74 m for the deep water case. The target location for the input wave packet is located 3 m downwave from the centre of the wavemaker source region. Two absorption beaches are then located at 1.5 m upwave and 5.5 m downwave from the source centre.

3.4.2. Boundary conditions

The front and back faces of the NWT, lying in the $x - z$ plane, are set to *empty*, indicating a 2D simulation. The bottom, left and right boundaries are set to a wall. The top boundary is set to atmospheric inlet/outlet condition.

3.4.3. Mesh

The mesh is depicted in Figure **??**. The mesh is one cell thick in the y direction, for implementation of the 2D simulation. Mesh refinement has been employed in the interface region leading to a cell size of 8 cells per A_0 and 100 cells per wave length. A grid convergence study has been performed to determine

Preprints (www.preprints.org) | NOT PEER-REVIEWED | Posted: 22 January 2019 doi:10.20944/preprints201901.0222.v1
Peer-reviewed version available at J. Mar. Sci. Eng. 2019, 7, 71; doi:10.3390/jmse7030071

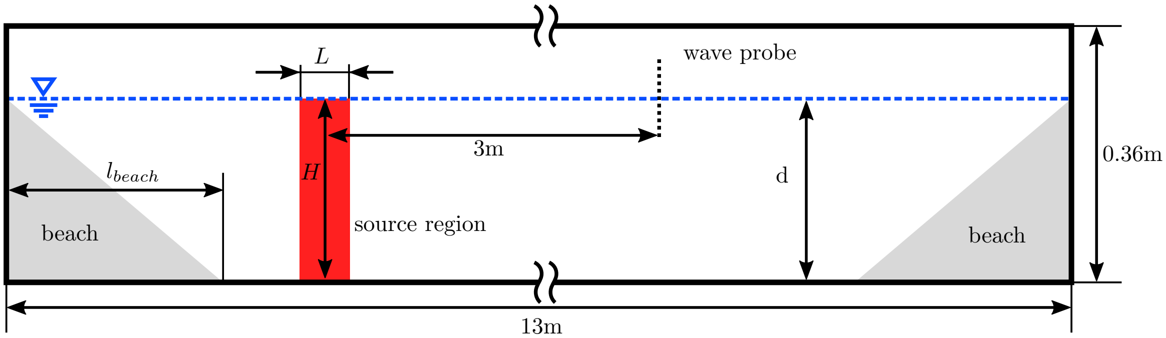

Figure 3. Schematic of the NWT including the main dimensions. For the shallow water cases the water depth d is set to 0.25m, for the deep water case is 0.74m

these sizes. Adjustable time stepping, based on a maximum allowable Courant number of 0.9, is used in all simulations.

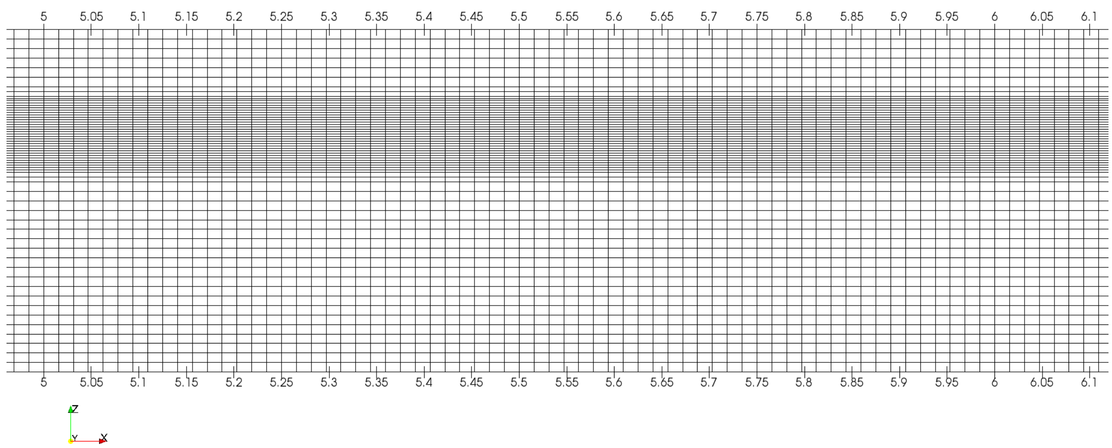

Figure 4. Snapshot of the NWT mesh, with refined region around the free surface. The grid resolution is kept constant in lateral directions

Preprints (www.preprints.org) | NOT PEER-REVIEWED | Posted: 22 January 2019 doi:10.20944/preprints201901.0222.v1

Peer-reviewed version available at J. Mar. Sci. Eng. 2019, 7, 71; doi:10.3390/jmse7030071

3.4.4. Calibration of the absorption beach

[?] recently published a method based on analytical theory to find the ideal magnitude of the damping parameter *sand* for monochromatic waves. In the future it will thus be possible to set the ideal damping parameters prior to each simulation. Herein, a parameter study is performed to investigate the absorption performance for the wave packet. Three different pairs of l_{beach} and $sand_{Max}$ were tested for the shallow water case, i.e. $l_{beach} = \lambda_p$ and $sand_{Max} = 5$; $l_{beach} = \lambda_p$ and $sand_{Max} = 7$, $l_{beach} = 2\lambda_p$ and $sand_{Max} = 6$. The first test, using $sand_{Max} = 5\text{s}^{-1}$ and $l_{beach} = \lambda_p$, yielded a reflection coefficient of 3.5%, with reflection evaluated using the method described in [?]. Increasing $sand_{Max}$ to 7s^{-1} results in a reflection coefficient of 2.5%; using $sand_{Max} = 6\text{s}^{-1}$ and $l_{beach} = 2\lambda_p$ reduced the reflection coefficient significantly to 0.2%. The latter beach configuration was then used in all subsequent cases. While even the first configuration, with a resulting reflection coefficient of 3.5%, is better than most experimental facilities [?] and many numerical methods, it highlights the flexibility of the approach. Larger beaches will invariably come with a greater computational cost but, for cases where very low reflection over a larger frequency range is required, they seem the only viable method. Fig **??** shows the definition of the dissipation parameter along the tank as used in the simulations.

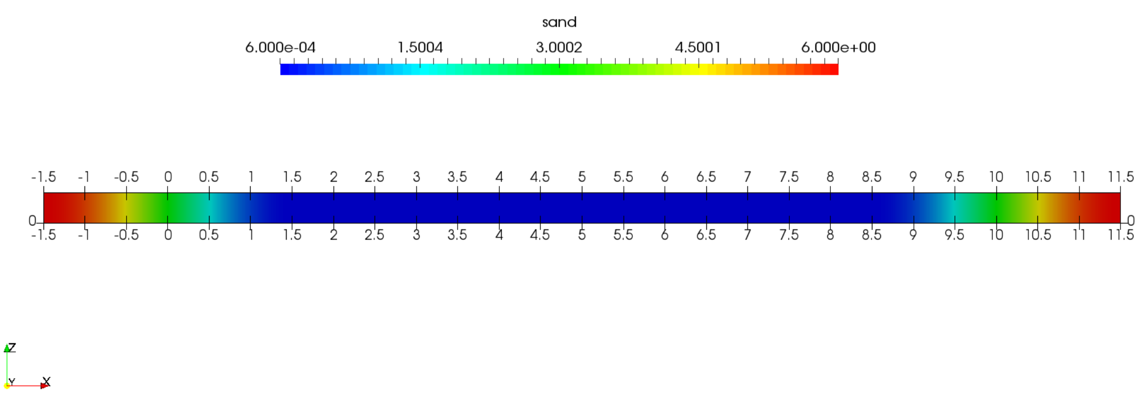

Figure 5. Gradually increasing damping factor *sand*. The grading depends on the location, with no damping (blue colour code) in the centre of the wave tank and highest damping (red colour code) at the far field boundaries

3.5. Source region test cases

120 muti-freqeuncy wave packet experiments were run in total, for 90 shallow water cases and 30 deep water cases, with varying source region layouts investigated. For the shallow water cases, simulations were run with the source region progressively centred at a third, a half, and two thirds of the water depth. For deep water cases, the centre of the source region is located at a depth of $\frac{\lambda_p}{4}$, or half the water depth. For each different source centre location, 30 experiments were run with varying source length region, L, of $0.125\lambda_p$, $0.25\lambda_p$, $0.5\lambda_p$, $1\lambda_p$, $1.25\lambda_p$ and varying height of the source region, H, of $0.125d$, $0.25d$, $0.5d$, $0.75d$, $1d$ and $1.25d$.

Preprints (www.preprints.org) | NOT PEER-REVIEWED | Posted: 22 January 2019 doi:10.20944/preprints201901.0222.v1

Peer-reviewed version available at J. Mar. Sci. Eng. 2019, 7, 71; doi:10.3390/jmse7030071

The performance of the various source region layouts is evaluated as the MSE between the target surface elevation, η_T, and the achieved result, η_R:

$$MSE = \frac{1}{K}\sum_{l}^{K}(\eta_{T,l} - \eta_{R,l})^2, \tag{6}$$

where K is the total number of time steps in the simulation.

4. Results and Discussion

In this section the case study results are presented and discussed. First, an example result from a single experiment (deep water case with source height of $\frac{\lambda_p}{8}$ and source length of $\frac{1}{4}\lambda_p$) is presented in Section **??**. The complete set of the results from all the shallow and deep water experiments are summarised in Sections **??** and **??**, respectively. Application of the simplified calibration method for regular waves is discussed in **??**.

4.1. Example result

Figure **??** displays an example of the typical decrease in MSE for increasing calibration iterations during an experiment. Note the evolution is non-monotonic, which is explained by Figure **??**, showing the corresponding surface elevation time traces from a selection of these calibration iterations. The first iteration is initialised with random input of small amplitude, and the resulting surface elevation is almost zero and the MSE of 3×10^{-5}, is large. The second iteration yields several waves with similar amplitude and frequency to the target wave packet, but out of phase, and the resulting MSE almost doubles. The fourth and fifth iterations decrease the MSE by orders of magnitude to 1×10^{-5} and 1×10^{-6} . The main peak of the wave packet is now already very well resolved and most of the error stems from some small high frequency waves after 11 s. Further iterations decrease the MSE to about 3×10^{-7}, agreement is now even good for the small ripples after 11 s. For all the results presented Sections **??** and **??**, 9 calibration iterations are used.

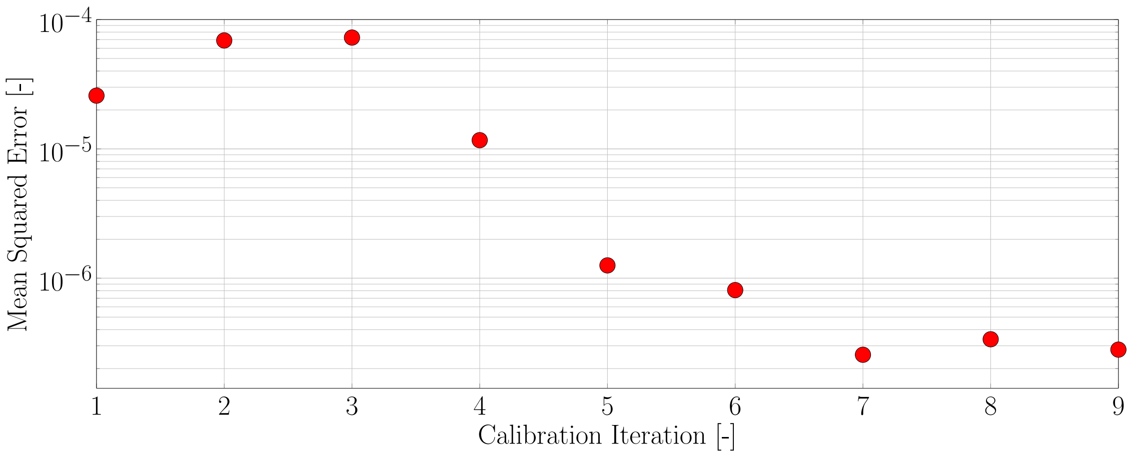

Figure 6. Example of the decrease in the MSE for increasing calibration iterations.

Preprints (www.preprints.org) | NOT PEER-REVIEWED | Posted: 22 January 2019 doi:10.20944/preprints201901.0222.v1

Peer-reviewed version available at J. Mar. Sci. Eng. 2019, 7, 71; doi:10.3390/jmse7030071

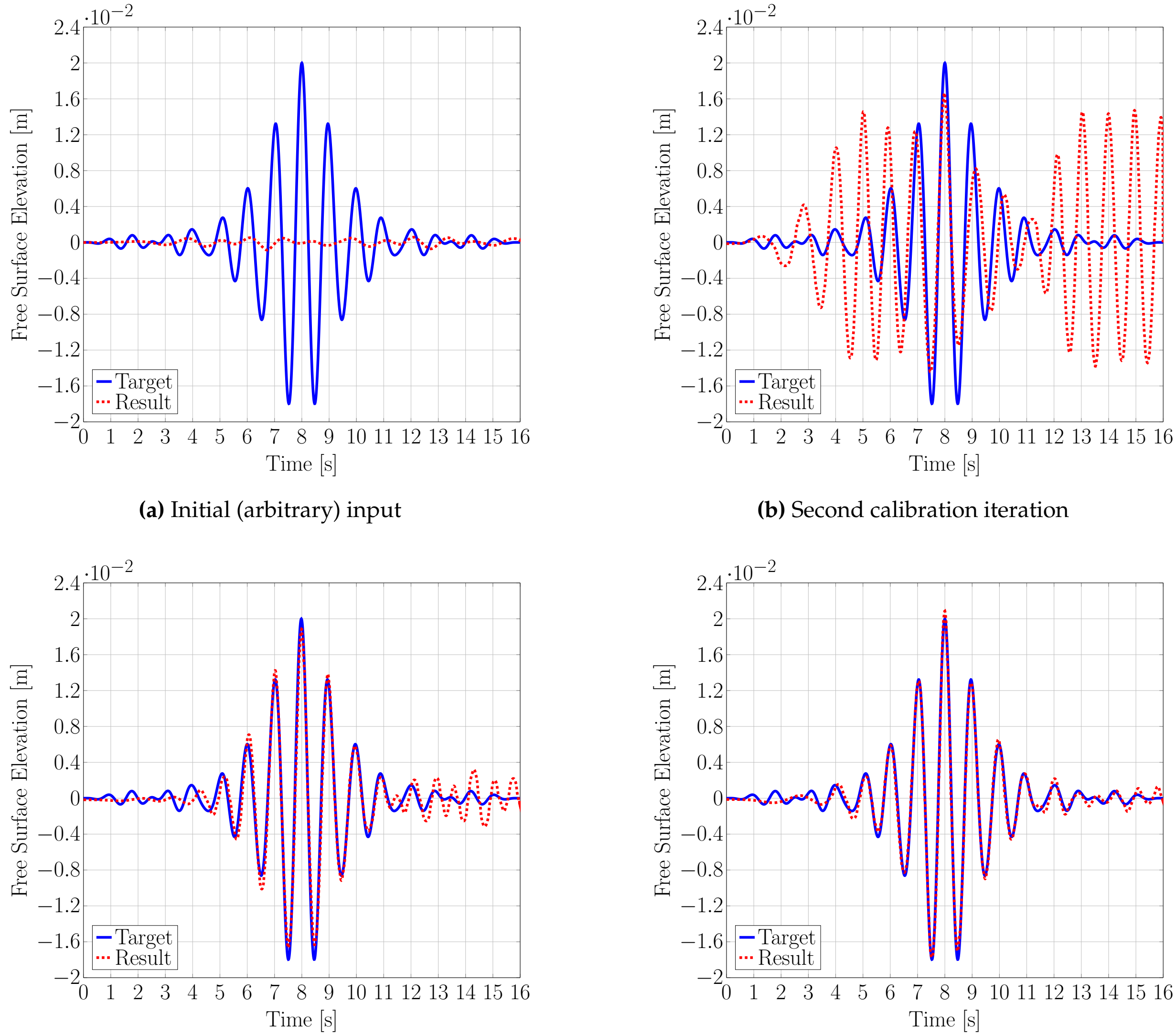

(a) Initial (arbitrary) input

(b) Second calibration iteration

(c) 5th calibration iteration

(d) Final calibration iteration

Figure 7. Example of the target and resulting surface elevation, at different calibration iterations, for the same case as Fig. **??**

4.2. Shallow water waves

The results from the shallow water experiments are summarised in Figures **??**, **??** and **??**, for the cases with the center of the source region at one third, one half and two thirds of the water depth, respectively. The results show that decreasing the length of the source region, from $1\lambda_p$ to $0.3\lambda_p$ or less, reduces the MSE by over two orders of magnitude. In contrast, the height of the source region is seen to have a much smaller influence on the wavemaker performance, with best results obtained when the source region spans over the entire water depth. Overall, the smallest MSE occurs for the experiment with the source region centred at half the water depth, the source length of $0.25\lambda_p$, and a source height of 1.25 times the water depth,

Preprints (www.preprints.org) | NOT PEER-REVIEWED | Posted: 22 January 2019 doi:10.20944/preprints201901.0222.v1

Peer-reviewed version available at J. Mar. Sci. Eng. 2019, 7, 71; doi:10.3390/jmse7030071

Figure **??** shows the target wave time series and the results of the experiments which produced the best results for the three different source centre depths. Variations between simulations are minimal. The centre of the wave packet is very well reproduced around its peak and the surrounding crests and troughs, with the main discrepancies occurring at the beginning and the end of the wave packet, with the CFD simulations presenting small amplitude ripples when the target wave is already reaching still water conditions.

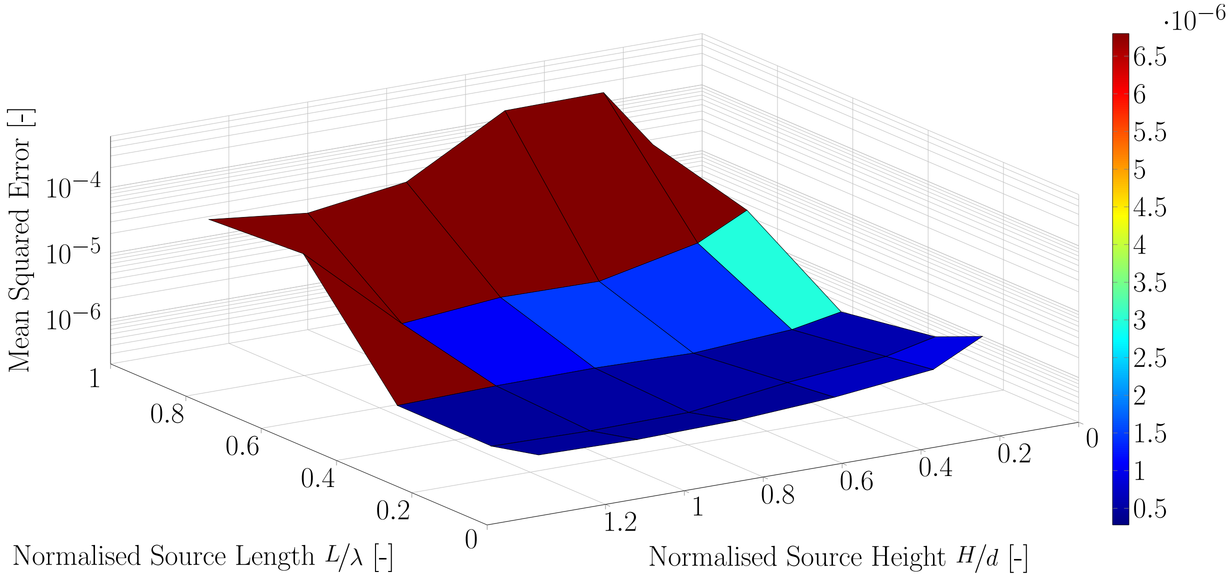

Figure 8. Shallow water case - Source centre at $\frac{d}{3}$: Minimal error (4.5×10^{-7}) for source height of $1d$ and source length $\frac{1}{4}\lambda_p$

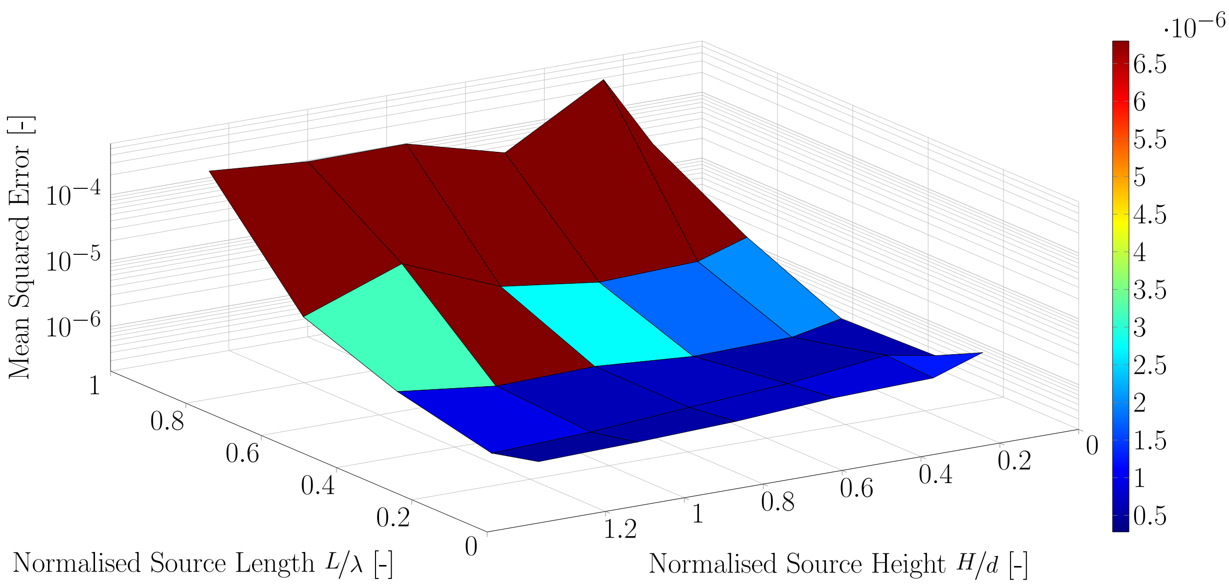

Figure 9. Shallow water case - Source centre at $\frac{d}{2}$: Minimal error (4.2×10^{-7}) for source height of $1.25d$ and source length $\frac{1}{4}\lambda_p$

Preprints (www.preprints.org) | NOT PEER-REVIEWED | Posted: 22 January 2019 doi:10.20944/preprints201901.0222.v1

Peer-reviewed version available at J. Mar. Sci. Eng. 2019, 7, 71; doi:10.3390/jmse7030071

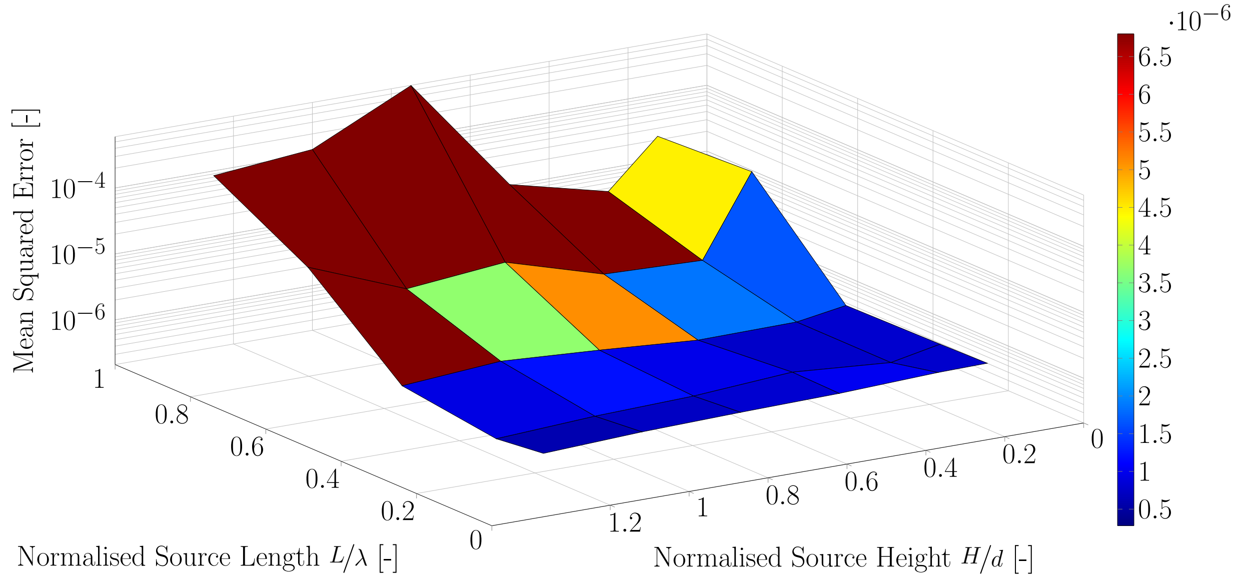

Figure 10. Shallow water case - Source centre at $\frac{2d}{3}$: Minimal error (5.9×10^{-7}) for source height of $1.25d$ and source length $\frac{1}{2}\lambda_p$

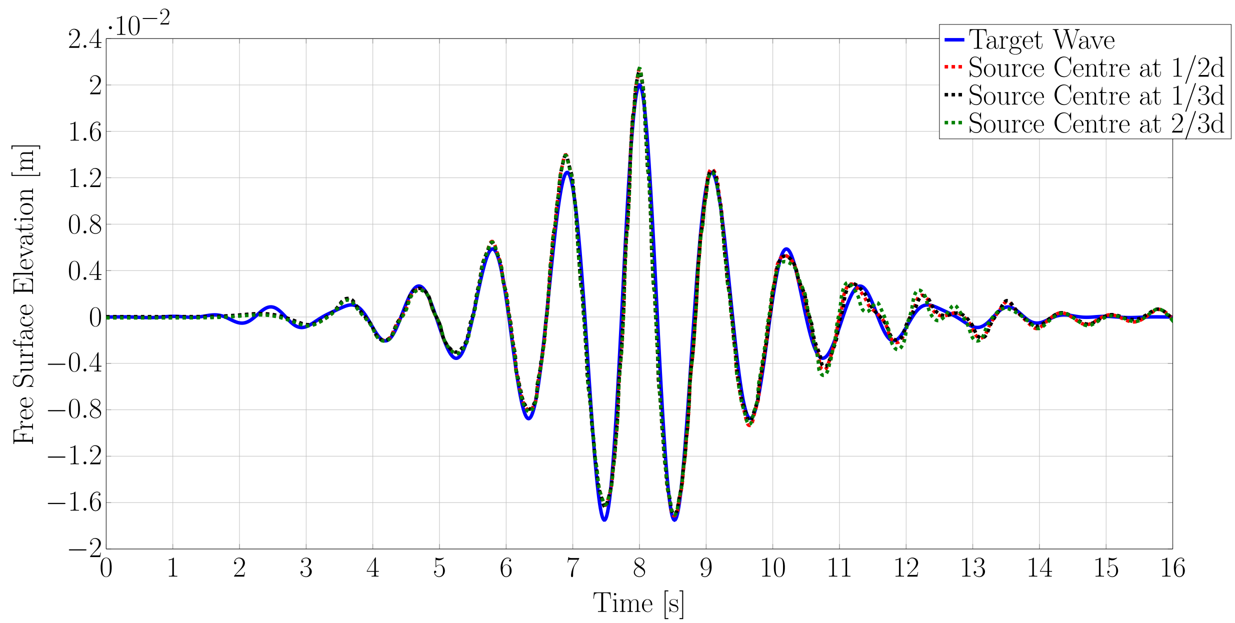

Figure 11. Surface elevation time series for shallow water experiments which produced the best results for the three different source centre locations

4.3. Deep water waves

Deep water waves only affect the water column up to a depth of half a wave length, it thus seems more appropriate to base the vertical position of the source region on that parameter. Because the source center position had little influence in the shallow water cases presented earlier, test cases were only run for varying source heights and lengths, with the source centre position fixed at $\lambda_p/4$.

Preprints (www.preprints.org) | NOT PEER-REVIEWED | Posted: 22 January 2019 doi:10.20944/preprints201901.0222.v1

Peer-reviewed version available at *J. Mar. Sci. Eng.* **2019**, *7*, 71; doi:10.3390/jmse7030071

Figure **??** shows the results from the deep water experiments. The minimum error is 2.8×10^{-7} for a source length of $0.25\lambda_p$ and height of 0.25 times the water depth, which is somewhat less than the best shallow water case. A wide range of source heights yields good results; only for small values of source heights, where the source region does not reach the surface, does the error increase significantly.

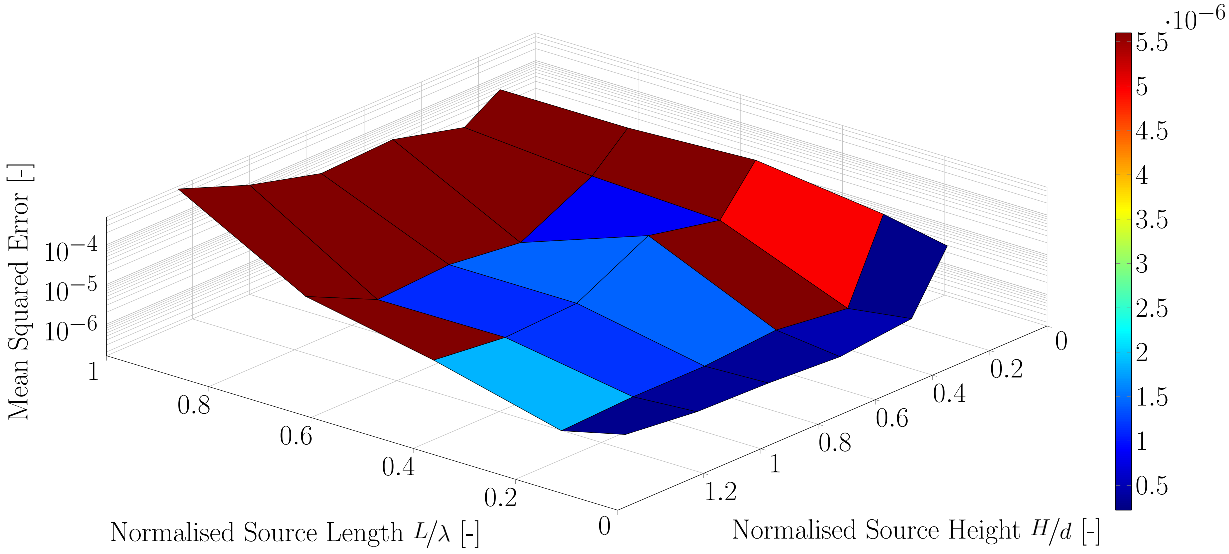

Figure 12. Deep water case: Minimal error ($5 \cdot 10^{-4}$) for source height of $\frac{\lambda_p}{8}$ and length $\frac{1}{4}\lambda_p$

4.4. Regular waves

Figure **??** shows the surface elevation during the first four calibration steps for deep and shallow water waves. In both cases the results converged rapidly, after the second iteration the results are almost identical for subsequent runs. Figure **??** shows the absolute difference between target wave height and the current value. For the second iteration errors are already within the millimetre range and decrease almost another order of magnitude in the third iteration, which can be deemed sufficient for any practical application.

Preprints (www.preprints.org) | NOT PEER-REVIEWED | Posted: 22 January 2019 doi:10.20944/preprints201901.0222.v1

Peer-reviewed version available at *J. Mar. Sci. Eng.* **2019**, *7*, 71; doi:10.3390/jmse7030071

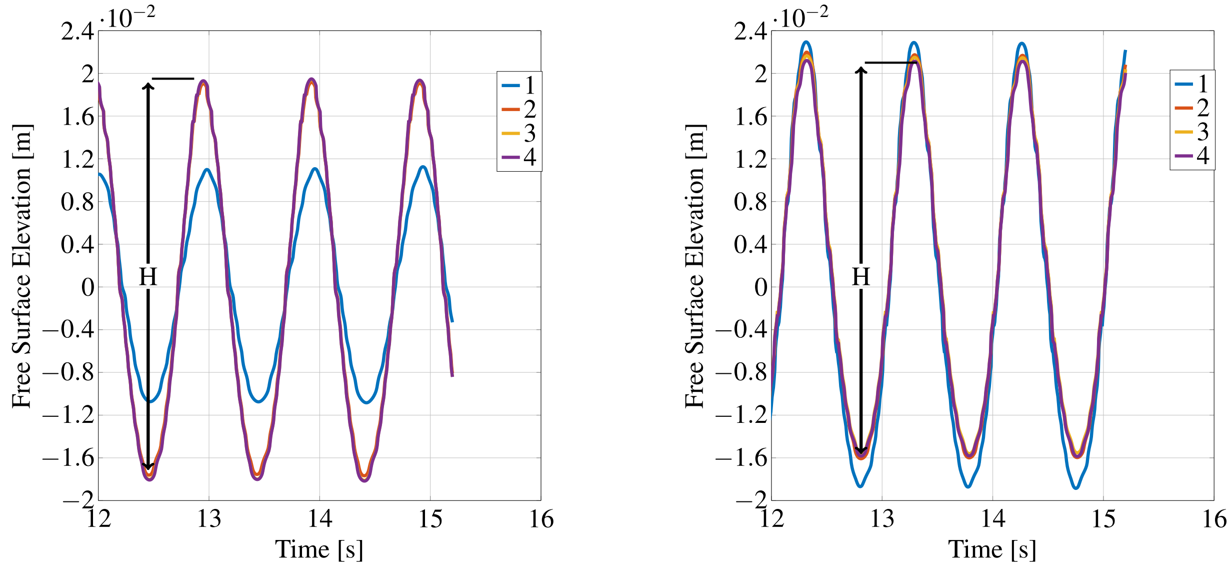

(a) Deep water. **(b)** Shallow water.

Figure 13. Surface elevation time series for regular waves. Numbers indicate the calibration iteration.

5. Conclusion

A NWM, based on the impulse source method, was implemented in the OpenFOAM framework. In combination with a calibration procedure, complex irregular wave patterns can be recreated in deep and shallow water, using an impulse source term acting in the horizontal direction. While the simple formulation of the source term facilitates implementation in the flow solver, the calibration procedure ensures that the target wave is created at the desired position and time in the NWT. Furthermore, reflection analysis demonstrates the ability of the numerical beach to achieve arbitrarily low reflection from boundaries and transparency of the wavemaker region. In the future, the work of [?] will allow to set the ideal beach parameters without the need to run parameter or calibration studies.

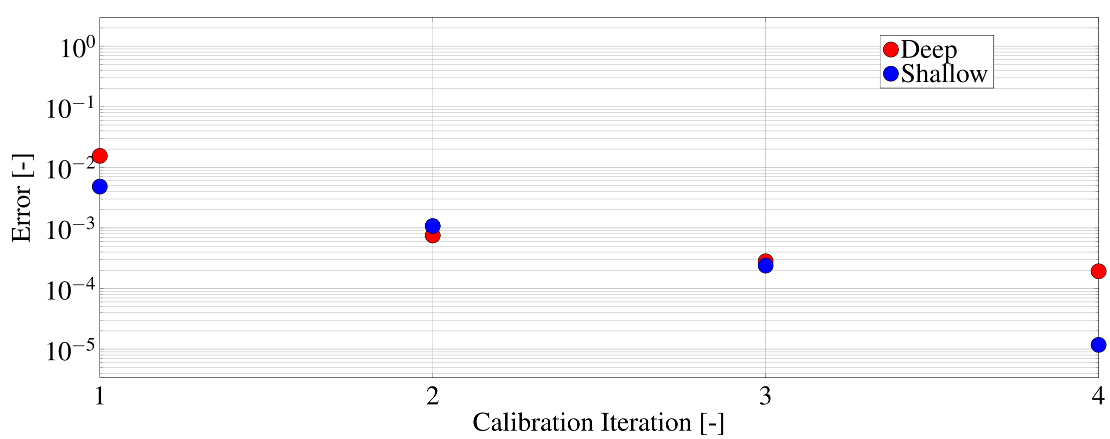

Figure 14. Error in wave amplitude versus numerber of calibration iterations.

Preprints (www.preprints.org) | NOT PEER-REVIEWED | Posted: 22 January 2019 doi:10.20944/preprints201901.0222.v1

Peer-reviewed version available at *J. Mar. Sci. Eng.* **2019**, *7*, 71; doi:10.3390/jmse7030071

Parameter sensitivity studies, investigating the effect of the shape and position of the wavemaker region, show that good results can be achieved over a wide range of parameters. For deep and shallow water, a wavemaker region length of less than a quarter of a wave length is suitable, which is less than recommended in previous work [**?**], and might enable the use of smaller computational domains. The vertical position of the centre of the wavemaker has overall little effect in shallow water conditions and good results were achieved if it was placed at half the water depth. For deep water cases, good results were obtained with the centre of the wavemaker at a quarter of a wave length below the surface. Even when starting from a poor initial parameter specification, the method is shown to converge to an accurate solution within a few iterations.

For monochromatic or regular waves, a simplified calibration method can be used. Tests show that the the amplitude can typically be found within four iterations.

Although the calibration method is standard in experimental test facilities, it can be expected to become inaccurate in higher order sea states. Improvements should be explored to take into account non-linear effects. A possible way forward might be neural networks of arbitrary complexity as described by [**?**].

Acknowledgements

This paper is based upon work supported by Science Foundation Ireland under Grant No. 13/IA/1886. Pál Schmitt's Ph.D. was made possible by an EPSRC Industrial Case Studentship 2008/09 Voucher 08002614 with industrial sponsorship from Aquamarine Power Ltd.

References